Journal of Power Sources 235 (2013) 95–104

Contents lists available at SciVerse ScienceDirect

Journal of Power Sources

journal homepage: www.elsevier.com/locate/jpowsour

Facile fabrication of multiwalled carbon nanotube/α-MnOOH coaxial nanocable films by electrophoretic deposition for supercapacitors

Hua Fang [a], Shichao Zhang [a,*], Xiaomeng Wu [a], Wenbo Liu [a], Bohua Wen [a], Zhijia Du [a], Tao Jiang [b]

[a] School of Materials Science and Engineering, Beihang University, XueYuan Road No. 37, HaiDian District, Beijing 100191, PR China
[b] Patent Examination Cooperation Center of the Patent Office, SIPO, Beijing 100083, PR China

HIGHLIGHTS

- Electrophoretic deposition of Multi-walled carbon nanotube/α-MnOOH coaxial nanocable films.
- 3D nanoporous network structure can facilitate fast ions and electron transportation.
- The films exhibit superior capacitive behaviors and cycle stability.
- Energy storage mechanism of MnOOH as supercapacitor electrode material is discussed.
- Their capacitive performances can be tuned by varying the deposition time.

GRAPHICAL ABSTRACT

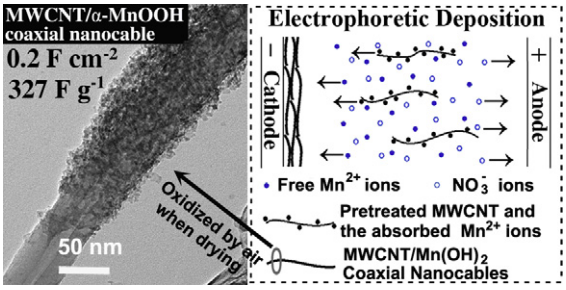

ARTICLE INFO

Article history:
Received 29 July 2012
Received in revised form
1 November 2012
Accepted 15 January 2013
Available online 14 February 2013

Keywords:
Supercapacitor
Manganese oxyhydroxide
Electrophoretic deposition
Coaxial nanocable
Multiwalled carbon nanotubes

ABSTRACT

Multiwalled carbon nanotube (MWCNT)/α-MnOOH coaxial nanocable (MMCNC) films are successfully fabricated by a simple and low-cost electrophoretic deposition (EPD) process. The as-prepared MMCNC films exhibit three-dimensional (3D) nanoporous network structure. A possible mechanism is proposed to explain the formation of the MMCNC films. Electrochemical test results show that the films exhibit superior capacitive behaviors and cycle stability in 0.1 M Na_2SO_4 aqueous solution. The thickness, mass loading and capacitive performance of the MMCNC films can be easily and continuously tuned by varying the deposition time. A relatively high mass specific capacitance of 327 F g^{-1} is obtained from the films with relatively low mass loading of 0.05 mg cm^{-2}, while, a relatively high areal capacitance of 0.2 F cm^{-2} is achieved when the mass loading was increased to 1.38 mg cm^{-2}. The superior capacitive performances can be attributed to the unique structure advantages of the MMCNC films. On one hand, the one-dimensional (1D) coaxial nanocable structure works, with MWCNT core serving as high electronic conductive frame and α-MnOOH sheath providing high pseudocapacitance. On the other hand, the 3D nanoporous network structure can facilitate fast ions transportation.

© 2013 Elsevier B.V. All rights reserved.

1. Introduction

Due to global fossil energy depletion and climate change, the exploitation of renewable sources such as the intermittent solar and wind has been hot issues of today's scientific community. For the same reason, the development of electric vehicles (EVs) and hybrid electric vehicles (HEVs) is facing a global booming at the moment. As a result, the electrochemical energy storage systems, such as batteries and supercapacitors, are expecting to play a larger part in our lives [1]. Owing to their high power density, high energy density and long cycle life, supercapacitors are believed to have

* Corresponding author. Tel./fax: +86 10 82338148.
E-mail address: csc@buaa.edu.cn (S. Zhang).

0378-7753/$ – see front matter © 2013 Elsevier B.V. All rights reserved.
http://dx.doi.org/10.1016/j.jpowsour.2013.01.195

potential to fill the power/energy gap between traditional dielectric capacitors and batteries/fuel cells [2]. Depending on the charge storage mechanism, supercapacitors are generally classified into two types: electrochemical double layer capacitors (EDLCs) and pseudocapacitors (also known as redox supercapacitors). EDLCs are based on porous carbon materials, characterized by better cycle stability and higher power density, while pseudocapacitors are based on pseudocapacitive materials such as metal oxides and conducting polymers, possessing higher energy density [3,4]. Recently, researches have focused on fabrication of composite materials composed of porous carbon materials and pseudocapacitive materials, expecting to obtain the combination of long cycle life stability, high power density and high energy density [1,2,5–8].

Manganese oxides in various forms seem to be one of the most promising electrode materials for supercapacitors because of their excellent reversibility, acceptable specific capacitance, low-cost and environmentally friendly characteristics [1]. Similar to manganese dioxide (MnO_2), manganese oxyhydroxide (MnOOH) also exhibits pseudocapacitive behaviors. Recently, γ-MnOOH nanorods are reported as material for supercapacitors and a relatively high specific capacitance 132 F g^{-1} was achieved [9]. As mentioned above, fabrication of the porous carbon/MnOOH composites could be one promising approach to improve the capacitive performances of MnOOH. However, graphene oxide/MnOOH nanowire composite has been prepared by hydrothermal reaction and explored as electrode material for supercapacitors, showing not high specific capacitance of 76 F g^{-1} [10]. Therefore, it remains a big challenge to synthesis novel porous carbon/MnOOH composites with excellent capacitive performance.

Among various carbonaceous materials (e.g. carbon nanotubes (CNTs), activated carbon, graphene, carbon aerogel, ordered mesoporous carbon), CNTs are ideal substrates for loading of pseudocapacitive materials because they can be easily processed into thin films. The CNT films can provide conductive frame for electron transport and three-dimensional (3D) nanoporous network structure for fast ions transportation [11,12]. Recently, electrochemical deposition of pseudocapacitive coatings (e.g. MnO_2 [11], V_2O_5 [12], NiO [13]) on the CNT film substrates have been reported and improved capacitive performances have been achieved. However, it's hard to obtain uniform oxide coating on the 3D nanoporous CNT frame through the entire film thickness, mainly due to the migration resistance of the ions. It is found that pseudocapacitive coatings are apt to grow on the outer surface of the CNT films, as the reported morphology in reference [14]. This phenomenon could be caused by the electromigration resistance of the electrolyte ions in CNT films. Excessive load of pseudocapacitive materials can block the opening pores in the CNT films, which results in the deterioration of electrochemical performances. To avoid damage to the nanoporous structure of CNT films, the mass loading of pseudocapacitive materials per area has to be limited. However, it is known that the mass loading per area is important for battery or supercapacitor devices and small mass loading per area could limit the practical applications of the composite films in supercapacitors [15]. Therefore, exploring novel process to produce uniform pseudocapacitive coating on the CNTs frame throughout the entire film thickness is a promising way to develop high performance electrode materials for supercapacitors.

Electrophoretic deposition (EPD) is an electrochemical method used to deposit charged colloidal particles onto conductive substrates. During the EPD process, the charged particles suspended in a suitable liquid move toward the oppositely charged electrode under the drive of a dc electric field and get deposited as a relatively compact and homogeneous film [16]. This technique has been known as a simple, versatile, low-cost, no need for binder, controllable film thickness and reliable room-temperature technique for the deposition of various solid particles on conductive substrates [16,17]. Recently, EPD technique has been developed for the fabrication of homogeneous composite films for supercapacitor application. Zhitomirsky et al. reported fabrication of composite films composed of MnO_2 and multiwalled carbon nanotubes (MWCNTs) by EPD from suspensions containing charged MnO_2 nanoparticles and MWCNTs [18–20]. The obtained composite films were nanoporous and showed far better capacitive performances than the pure MnO_2 films. Later, Xiao et al. [21] prepared the MWCNT/MnO_2 composite by in-situ redox reaction. Then, the obtained MWCNT/MnO_2 composites were dispersed into ethanol and EPD experiment was carried out to fabricate MWCNT/MnO_2 composites films for supercapacitor. More recently, similar EPD of the MnO_2-coated MWCNTs on a flexible graphite sheet was reported, and the resulted composite films showed a high specific capacitance of 443 F g^{-1} [22]. Thus, EPD technique has been proved to effective in fabricating homogeneous composite films for supercapacitor applications. However, the above mentioned EPD procedures usually involve multi-steps and some of the steps are not easy to perform, which might inevitably increase the cost. Since one of the main advantages of manganese oxides is their low cost, it is vital to develop simple and low cost synthetic route for fabrication of manganese oxides/CNT composite materials.

Several recent researches indicate that controlled electrochemical redox reactions could occur in the EPD process. Firstly, Du and Pan reported the preparation of high power density MWCNT films for supercapacitors by EPD method from MWCNT ethanol suspension which contained $Mg(NO_3)_2$ as the charge additive [23]. It has been demonstrated that $Mg(OH)_2$ was deposited on the cathode during the EPD process via a water electrolysis induced deposition of Mg^{2+} ions. The resulted $Mg(OH)_2$ matrix could improve the adhesive strength between MWCNT particles and the nickel foil substrate, leading to improved capacitive performances. Secondly, Ni-decorated MWCNT films were deposited onto stainless steel substrates by a similar EPD process from MWCNT isopropyl alcohol suspension which contained $Ni(NO_3)_2$ as the charge additive [24]. The proposed mechanism was that Ni^{2+} ions adsorbed on the MWCNTs were reduced to form metallic Ni as soon as the MWCNTs arrived at the substrate, because the high electrical conductivity of MWCNTs allows electron to conduct from the conductive substrate to the outer layer of MWCNTs. Based the above mentioned results, EPD technique can be directly used for facile one-step fabrication of functional composite films by tuning the composition of the EPD suspension.

In this research, EPD experiments are carried out from MWCNT ethanol suspension which contains $Mn(NO_3)_2$ as the charge additive. Excitingly, characterization results show that homogeneous MWCNT/α-MnOOH coaxial nanocable (MMCNC) films are successfully fabricated, with uniform α-MnOOH coating on the MWCNT frame throughout the entire film thickness. The obtained MMCNC films show a 3D nanoporous network structure and superior electrochemical capacitive performances.

2. Experimental

MWCNTs were purchased from Chengdu Organic Chemicals Co. Ltd. (Chengdu, China). The outer diameter and length of the MWCNTs were reported to be ~50 nm and 0.5–2 μm, respectively. For purification and functionalization, MWCNTs were pretreated by refluxing in boiling concentrated nitric acid for 6 h, followed by washing with deionized water and then drying at 60 °C. Absolute ethanol (AR), concentrated nitric acid (AR) and 50% $Mn(NO_3)_2$ aqueous solution (AR) were used as received.

2.1. Synthesis of MMCNC films by EPD

In a typical EPD experiment, 6.5 mg of pretreated MWCNTs was dispersed in 50 mL of absolute ethanol by ultrasonication. Then, 0.01–0.1 g 50% $Mn(NO_3)_2$ aqueous solution was dissolved into the suspension. A nickel foil (15 mm × 15 mm) and a platinum foil (15 mm × 15 mm) were put into the suspension and kept parallel as the EPD cathode and anode, respectively. A dc voltage of 50 V was applied on the EPD electrodes and thus the positively charged MWCNTs were attracted toward the nickel foil cathode. After the electrophoresis, the as-prepared EPD films were washed with absolute ethanol, dried at room temperature and then heat treated in an oven at 200 °C for 2 h under ambient air environment. It should be mentioned that the samples used for most characterization were prepared with a deposition time of 150 s. However, in order to increase the areal mass loading (mass loading per unit area, mg cm^{-2}) and areal capacitance (capacitance per unit area, F cm^{-2}), large number of MMCNC films were prepared with prolonged deposition time ranging from 30 s to 900 s, which were specifically marked. The mass loading of the MMCNC films under different deposition time was carefully measured by weighing the nickel foil before and after EPD experiment.

For comparison, bare MWCNT films without α-MnOOH coating were also prepared by EPD technique according the report [23]. The fabrication process was the same as that for the MMCNC films except that the charge additives of $Mn(NO_3)_2$ was substituted by $Mg(NO_3)_2$ with much lower concentration. The deposition time was also 150 s.

2.2. Characterization of the samples

Morphologies and microstructures of the MMCNC films were characterized by filed-emission scanning electron microscopy (FE-SEM, Hitachi, S-4800), transmission electron microscopy (TEM) and high-resolution TEM (HRTEM, JEOL 2010), and X-ray diffraction patterns (XRD, Rigaku D/Max-2400) with Cu Kα radiation. Oxidation state and composition of the α-MnOOH sheath were investigated by X-ray photoelectron spectroscopy (XPS) using an AXIS Ultra instrument from Kratos Analytical. To measure the actual content of MWCNTs in the MMCNC films, thermogravimetric (TG) analysis was carried out in air (25 mL min^{-1}, 25–900 °C, 10 °C min^{-1}) using a simultaneous thermal analyzer (NETZSCH STA 449C).

2.3. Electrochemical measurements

To investigate the electrochemical properties of the MMCNC films, cyclic voltammetry (CV) tests were made using an Im6-ex electrochemical workstation (Zahner. Inc. Germ). The scan rate used for CV tests ranged from 5 to 50 mV s^{-1}. Galvanostatic charge/discharge (GCD) tests were performed with current densities ranging from 0.2 to 5 mA cm^{-2} by using a MSTAT8 battery test system (Arbin Instruments). All the electrochemical measurements were done in 0.1 M Na_2SO_4 aqueous solution by using a 3-electrode system, with a voltage range of 0–0.85 V (vs. SCE). The MMCNC films were used as the working electrodes, a platinum plate as the counter electrode, and a saturated calomel electrode (SCE) as the reference electrode. For comparison, the bare MWCNT films were also tested using the same methods.

3. Results and discussion

3.1. Synthesis mechanism

Fig. 1 illustrates the process for preparing the MMCNC films. Before EPD experiments, MWCNTs are pretreated by refluxing in boiling concentrated nitric acid. This pretreatment is known to create oxygen-containing surface functional groups on the chemically inert surface of MWCNTs, thus facilitating good dispersion of MWCNTs, uniform distribution of absorbed ions and finally uniform coatings [25]. In the EPD suspension, the dispersed MWCNTs are positively charged due to the surface adsorption of Mn^{2+} ions. During the EPD process, positively charged MWCNTs, together with the absorbed Mn^{2+} ions and the free Mn^{2+} ions, move toward the cathode under the drive of the electric field as shown in Fig. 1. As soon as the MWCNTs arrive at the substrate, they instantly act as micro-cathodes because their excellent electrical conductivity allows electrons to transfer from the nickel foil to their outside surface [24]. Thus, cathodic electrolysis of H_2O and reduction of NO_3^- could occur on the outside surface of MWCNTs, both of which can produce OH^- species near the MWCNT/suspension interface. The so-generated local pH increase leads to the fast deposition of the absorbed Mn^{2+} ions and the free Mn^{2+} ions in the vicinity of the MWCNT/suspension interface as well, resulting in uniform $Mn(OH)_2$ coatings on the sidewall of the deposited MWCNTs. As a result, $Mn(OH)_2$/MWCNT coaxial nanocables are formed. The above mentioned reaction mechanism can be expressed by the following

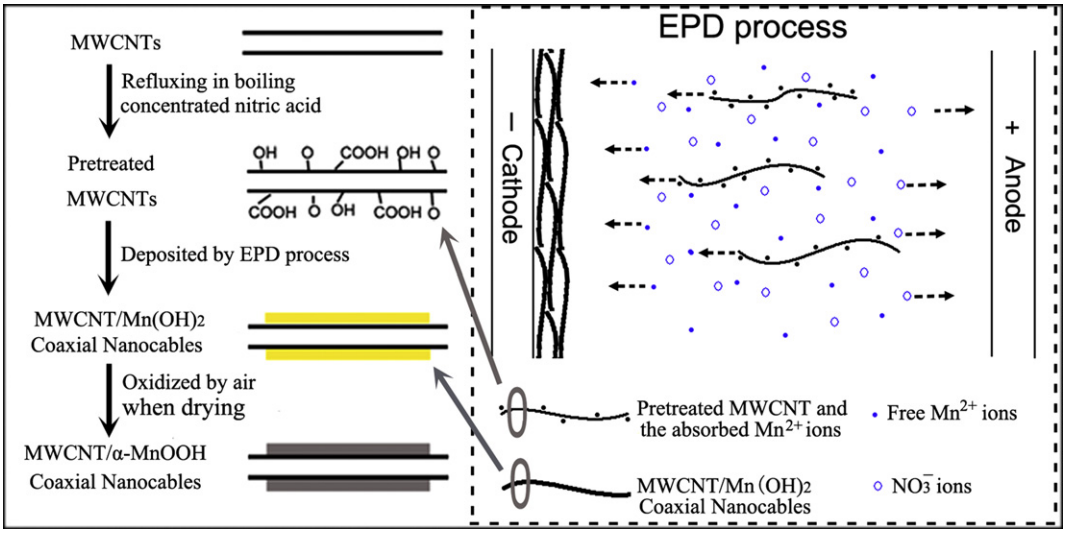

Fig. 1. The schematic diagram of the process for preparing the MMCNC films.

reactions, which is proposed by analogy to the reported cathodic reactions in the EPD process [23,26].

$$NO_3^- + H_2O + 2e^- = NO_2^- + 2OH^- \quad (1)$$

$$2H_2O + 2e^- = 2OH^- + H_2 \quad (2)$$

$$Mn^{2+} + 2OH^- = Mn(OH)_2 \quad (3)$$

As the EPD process going on, MWCNTs continuously get deposited on the cathode. Compared with the early arrived MWCNTs that have already been coated with $Mn(OH)_2$ sheath, the newly arrived MWCNTs uncoated with $Mn(OH)_2$ are more close to the bulk EPD suspension and more electric conductive. Therefore, the newly arrived MWCNTs are bound to successively replace the early arrived MWCNTs to provide active MWCNT/suspension interface for the above mentioned cathodic reactions. As a result, all the MWCNTs deposited on the cathode can be coated with $Mn(OH)_2$ sheath consecutively in the order of arrival-time sequence. That is to say, EPD of MWCNTs on the nickel substrate and growth of $Mn(OH)_2$ sheath on MWCNT sidewall can be carried out synchronously in the EPD process, resulting in uniform $Mn(OH)_2$ sheath coated on the MWCNT frame through the entire film thickness.

$Mn(OH)_2$ is reported to be highly unstable in presence of oxygen and can be readily oxidized to various manganese oxides, such as MnO_2, Mn_2O_3, MnOOH, Mn_3O_4, depending on the oxidizing atmosphere [27–30]. Recently, Liu et al. reported cathodic deposition of mesoporous hydrous MnO_2 nanowall arrays [31,32]. The proposed mechanism is a similar water electrolysis induced precipitation of $Mn(OH)_2$ and the following oxidation of $Mn(OH)_2$ by air in the drying process. However, the oxidation product of the $Mn(OH)_2$ sheath after drying at 200 °C under air atmosphere is proved to be α-MnOOH under our experimental conditions. As a result, the MMCNC films with 3D nanoporous network structure are obtained.

3.2. Surface morphology and microstructure characterizations

The MMCNC films used for characterization are prepared with a deposition time of 150 s, of which the areal mass loading is ~0.31 mg cm^{-2} Fig. 2 shows the typical morphology and microstructure of the MMCNC films. As shown in Fig. 2a, the obtained films present a 3D nanoporous network structure composed of one-dimensional (1D) MMCNCs. The coaxial nanocables are ~80 nm in diameter, much larger than that of the neat MWCNTs. The increase in diameter indicates the successful coating of the α-MnOOH sheath on the sidewall of the MWCNTs. As shown in Fig. 2b, the films are nanoporous through the entire film thickness. Such an open porous network structure can facilitate easy access of the solvated ions to the electrode/electrolyte interface. The TEM image of a single MMCNC with broken α-MnOOH sheath is shown in Fig. 2c, from which the core MWCNT and the α-MnOOH sheath can be easily distinguished by their morphologies. The α-MnOOH sheath is very uniform, with thickness of ~15 nm.

Inset of Fig. 2c presents a typical selected area electron diffraction (SAED) pattern with a set of diffused concentric rings, proving the polycrystalline nature of the α-MnOOH sheath. The d-spacings obtained from the rings are 0.35, 0.27, 0.23 and 0.16 nm, which can be assigned to the (120), (040), (200) and (151) planes of groutite α-MnOOH (JCPDS# 120733), respectively. In the HRTEM image shown in Fig. 2d, the observed lattice fringes with d-spacing of 0.21 nm are also belonged to the (220) plane of groutite, α-MnOOH. By adjusting the focal length we can get a clear image of the lattice fringes belonging to MWCNTs, which is shown in the inset of

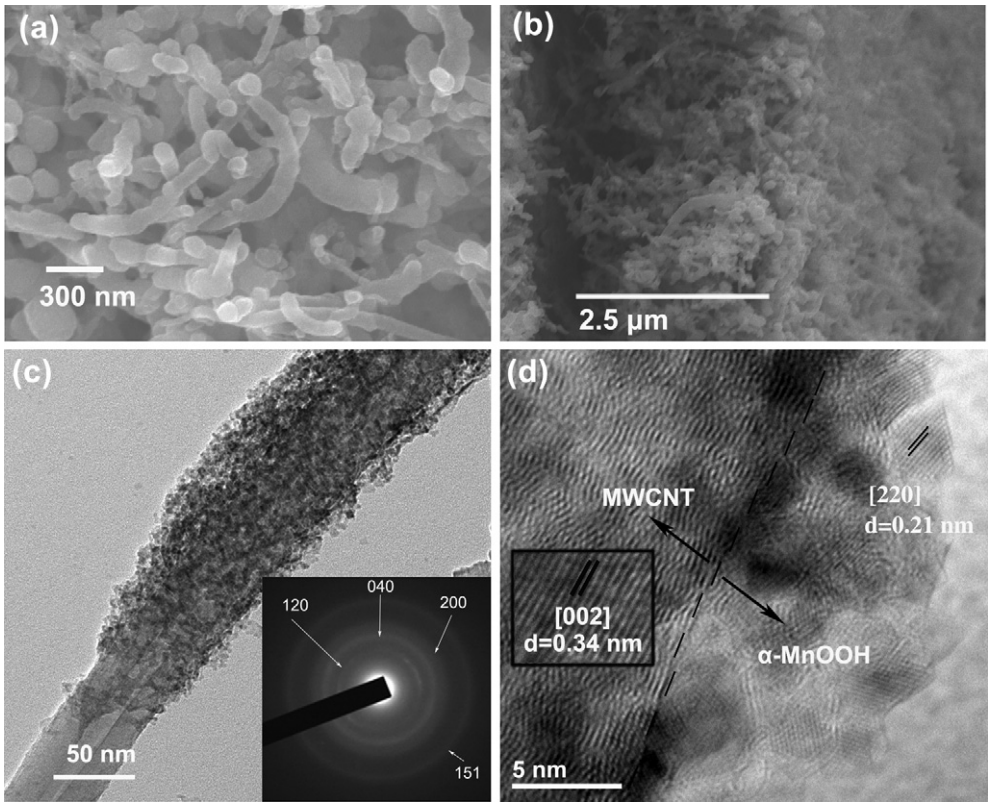

Fig. 2. (a) Surface and (b) cross-section SEM images of the MMCNC films; (c) TEM image of single MMCNC with broken α-MnOOH sheath (inset shows the SAED pattern of α-MnOOH sheath) and (d) HRTEM image of the MMCNC (the lattice fringes shown inset corresponding to the (002) planes of MWCNTs).

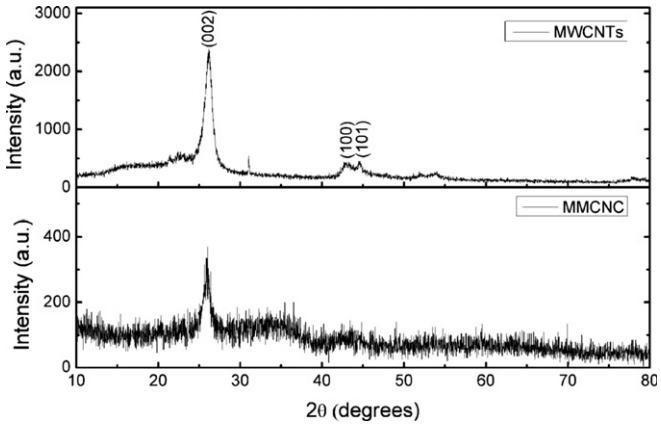

Fig. 3. XRD patterns of the neat MWCNTs and the MMCNC films.

Fig. 2d. The lattice fringes with a d-spacing of 0.34 nm are very clear, corresponding to the (002) plane of MWCNTs.

The neat MWCNTs and the MMCNC films were further characterized by XRD to check their phase composition. As shown in Fig. 3, both the neat MWCNTs and the MMCNC films show the (002) diffraction peak of MWCNTs at $2\theta = 26.2°$, corresponding to the d-spacing of 0.342 nm which have been observed by the HRTEM shown in the inset of Fig. 2d. The (002) diffraction peak from the MMCNC films is much weaker than that from the neat MWCNTs, indicating the successfully fabrication of the MWCNT based composite. However, no obvious diffraction peak emerges corresponding to the structure of α-MnOOH phase, indicating the low level of crystallinity. As a result, it's hard to characterize the phase of the α-MnOOH sheath through the XRD measurement.

Table 1
O(1s) Multiplet branching ratios for XPS spectra of the MMCNC films.

Name	Peak position (eV)	Area	Percentage[a] (%)
Mn–O–Mn	529.78	48440.4	47.8
Mn–O–H	531.25	47099.3	46.5
H–O–H	532.58	5707.0	5.6

[a] The percentage represents the contribution of each peak to the total number of counts under the O(1s) peak.

3.3. XPS analysis

The composition and oxidation state of the MMCNC films were analyzed by XPS spectroscopy. As shown in Fig. 4a, the Mn 3s XPS spectrum splits into a doublet of peaks. The multiplet splitting energy (ΔE) is reported to increase linearly as the valence of Mn element (n, $2 \leq n \leq 4$) decreases following the equation of $\Delta E \approx 7.88 - 0.85n$ [33]. The measured ΔE is about 5.37 eV and the calculated valence of Mn atoms is ~3.

As is presented in Fig. 4b, the O 1s XPS spectrum of the MMCNC films has a maximum near 529.8 eV, a distinct shoulder near 531.3 eV and a pronounced tail centered near 532.6 eV, corresponding to three different types of oxygen bonds: Mn–O–Mn, Mn–O–H, and H–O–H, respectively [34]. The shape and peak

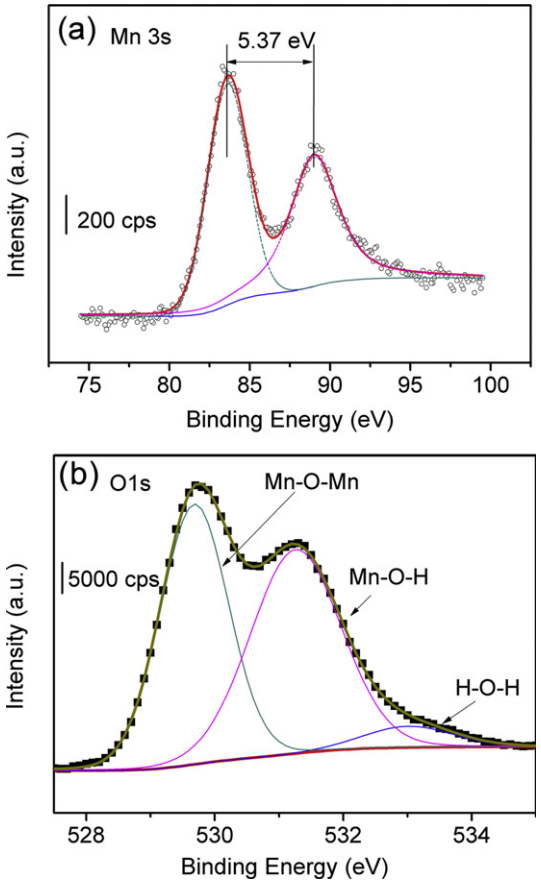

Fig. 4. (a) Mn 3s and (b) O 1s XPS spectra of the MMCNC films.

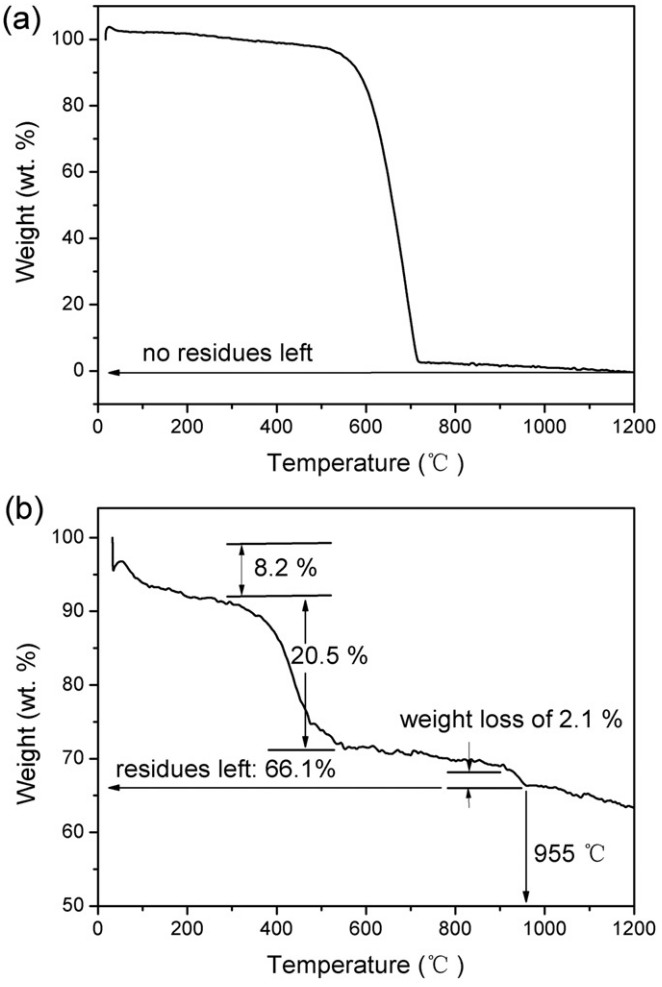

Fig. 5. TG analysis of (a) neat MWCNTs and (b) MMCNC films.

positions of the O 1s XPS spectrum are in good agreement with that of the previously reported MnOOH [35,36]. The Gaussian fitting of the O(1s) XPS spectrum is carried out by using a XPS peak fitting program named XPSPEAK (version 4.0). The obtained peak positions, areas and relative intensities are listed in Table 1. The oxygen bond Mn–O–Mn and Mn–O–H show almost equal contributions to the O 1s XPS spectrum, indicating almost equal abundance of oxide (O^{2-}) and hydroxide (OH^-) and thus idealized MnOOH composition [35,36]. The existence of H–O–H spectra can be attributed to any physisorbed and chemisorbed H_2O species.

3.4. TG analysis

The mass percentage content of MWCNTs in the MMCNC films was estimated from the TG results. As presented in Fig. 5a, neat MWCNTs are stable up to 550 °C and become completely decomposed above 750 °C, agreeing well with the previous report [37]. However, there is no visible weight loss between 550 and 750 °C in Fig. 5b. It can be inferred that the MWCNTs in the composite films begin to decompose at a much lower temperature, which may be caused by the catalytic effect of the α-MnOOH sheath. As shown in Fig. 5b, the 8.2% weight loss between 30 and 200 °C may be resulted from the loss of physisorbed and chemisorbed water. According to the literature, MnOOH should have three weight loss peaks with inflexion point 250, 556 and 943 °C which correspond to the formation of MnO_2, Mn_2O_3 and Mn_3O_4, respectively [38]. Thus, the weight loss of 20.5% between 200 and 600 °C in Fig. 5b may be resulted from the transformation of MnOOH to MnO_2 and Mn_2O_3, and the decomposition of MWCNTs. Only the weight loss of about 2.1% between 910 and 955 °C is distinguishable in Fig. 5b, corresponding to the transformation from Mn_2O_3 to Mn_3O_4. It is reasonable to assume that the residue of 66.1% at 955 °C can be attributed to pure Mn_3O_4 because all oxides and hydroxides of manganese can be transformed to Mn_3O_4 if heated in air to about 1000 °C [28]. Then, the weight content of the α-MnOOH shell in the composite film can be calculated as 76.2% based on the law of conservation of mass. Based on the above analyses, the weight content of MWCNTs can be estimated to be 15.6% (100% − 76.2% − 8.2% = 15.6%).

3.5. Electrochemical behavior of the MMCNC films

CV and GCD tests were carried out to investigate the capacitive performance of the MMCNC films. For comparison, the bare MWCNT films were also tested. As shown in Fig. 6a, the CV curve of the MMCNC film shows nearly rectangular shape, indicating ideal capacitive behavior. Compared with that of the bare MWCNT films, the much larger response current of the MMCNC films corresponds to larger capacitance. Fig. 6b shows the CV curves of the MMCNC films at different scan rates ranging from 5 to 50 mV s^{-1}. Nearly rectangular shapes are observed at all scan rates, which indicates the good power performance of the MMCNC films.

The Fig. 6c presents the typical GCD curves of the MMCNC films obtained at different GCD current densities ranging from 0.2 to 5 mA cm^{-2} (or from ≈0.65 to ≈16.1 A g^{-1}). The similar triangular shapes demonstrate high power performance of the MMCNC films. The specific capacitances of the MMCNC films are calculated from the GCD test results based on the total mass of α-MnOOH sheath and MWCNT core by using the equation of $C_m = (I \times \Delta t)/(\Delta U \times m)$, where the C_m, I, Δt, ΔU and m are the mass specific capacitance (F g^{-1}), GCD current (A), discharge time (s), GCD voltage window (0.85 V) and mass loading of the MMCNC film (g), respectively. As is shown in Fig. 6d, the specific capacitance of the MMCNC films reaches 202 F g^{-1} at 0.2 mA cm^{-2} (or ≈0.65 A g^{-1}). When the

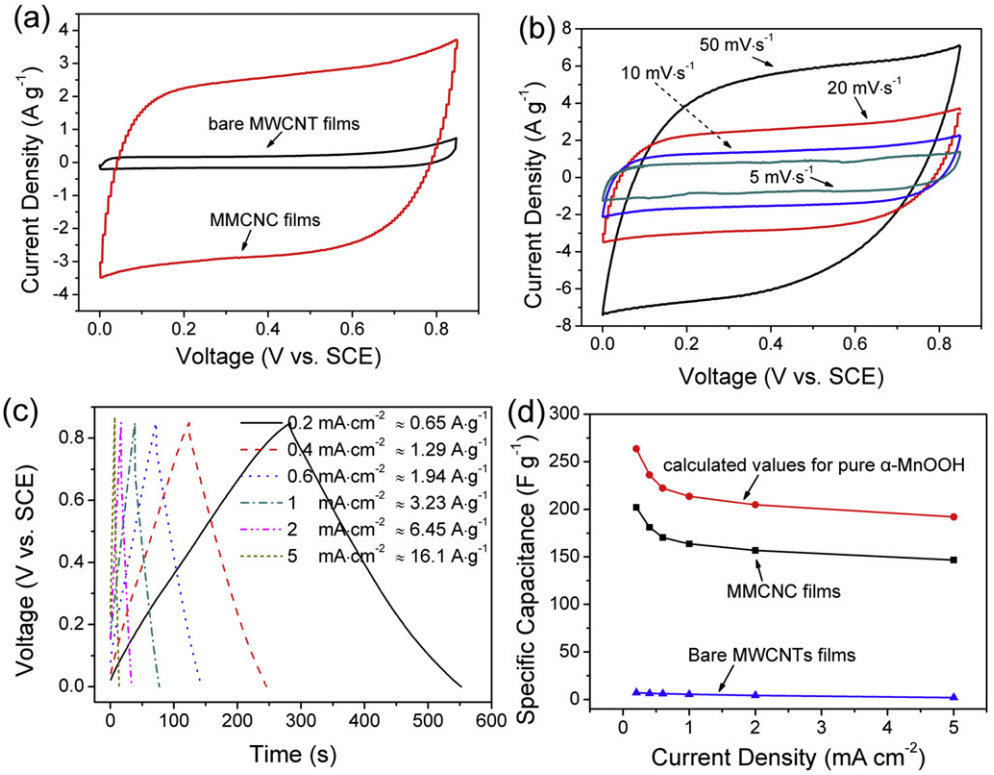

Fig. 6. (a) CVs curves of the MMWCNC films and the bare MWCNT films at 20 mV s^{-1}; (b) CV curves of the MMCNC films at different scan rates ranging from 5 mV s^{-1} to 50 mV s^{-1}. (c) GCD curves of the MMCNC films at different GCD current densities. (d) Specific capacitance of the MMCNC films and the bare MWCNT films, and the calculated specific capacitance from the α-MnOOH shealth at different GCD current densities.

current density increases to 5 mA cm^{-2} (or ≈16.1 A g^{-1}), the specific capacitance reduced to 147 F g^{-1}, retaining ~73% of that at 0.2 mA cm^{-2}.

The specific capacitance from the α-MnOOH shell can be estimated according to the weight percentage of the α-MnOOH (76.2 wt.%) in the total MMCNC film by using the equation of $C_{MnOOH} = (m \times C_m - 15.6\% \times m \times C_{MWCNT})/(76.2\% \times m)$, where C_{MnOOH} and C_{MWCNT} are the calculated mass specific capacitance of the α-MnOOH sheath (F g^{-1}) and the mass specific capacitance of the pretreated MWCNTs (F g^{-1}), respectively. At a current density of 0.2 mA cm^{-2}, the specific capacitance of the pretreated MWCNTs is only ~7 F g^{-1}. The counterpart of the MMCNC film is 202 F g^{-1}, nearly thirty-fold greater than that of the bare MWNTs electrode. The calculated specific capacitance for α-MnOOH is 264 F g^{-1} at a current density of 0.2 mA cm^{-2}. It should be mentioned that, for simple and for practical application purpose, the reported mass specific capacitances in the following part of this research are calculated based on the total weight of the MMCNC films.

The cycle performance of the MMCNC films was tested by GCD cycles at a GCD current density of 0.2 mA cm^{-2} (or ≈0.65 A g^{-1}) and the typical test result is shown in Fig. 7a. The initial capacitance of the MMCNC film reaches 202 F g^{-1} and shows a slight increase in capacitance in the initial stage of the GCD cycles. After 260 cycles, the specific capacitance increases to 211 F g^{-1} and then remains stable. After 1200 cycles, the specific capacitance still retains 205 F g^{-1}, exhibiting excellent long cycle life stability. Typical morphology of the MMCNC films which have experienced 1200 GCD cycles is shown in Fig. 7b. The 3D nanoporous network structure of the MMCNC films is retained, demonstrating that the coaxial nanocable structure can endure long GCD cycles. It is noteworthy that the α-MnOOH sheath becomes more nanoporous after the GCD cycles. The nanoporous sheath can provide larger

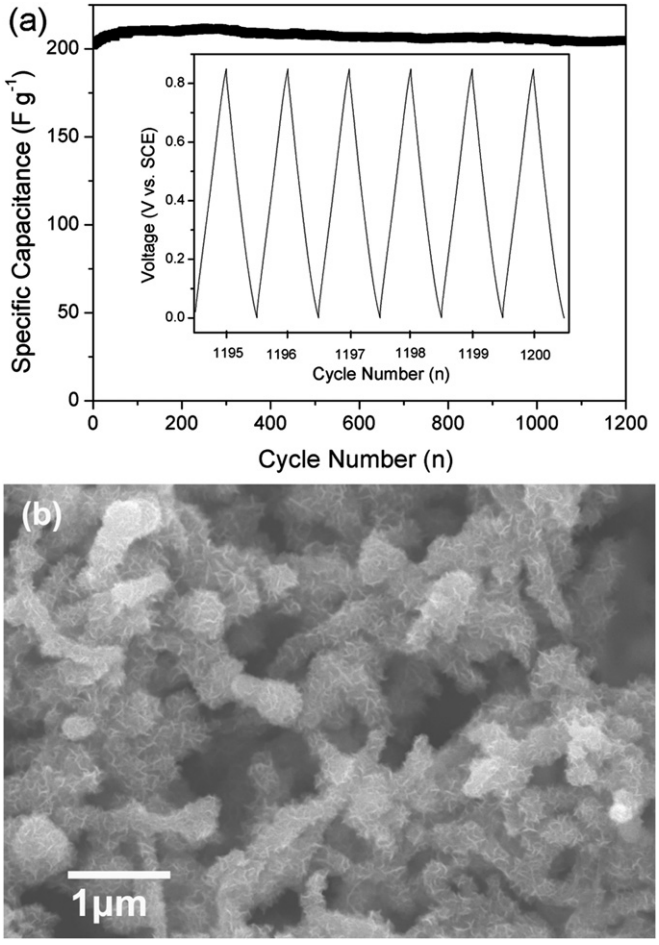

Fig. 7. (a) Cycling stability of the MMCNC film at a GCD current density of 0.2 mA cm^{-2}, inset shows the GCD curves form cycle 1195–1200. (b) SEM image of the MMCNC film after 1200 GCD cycles.

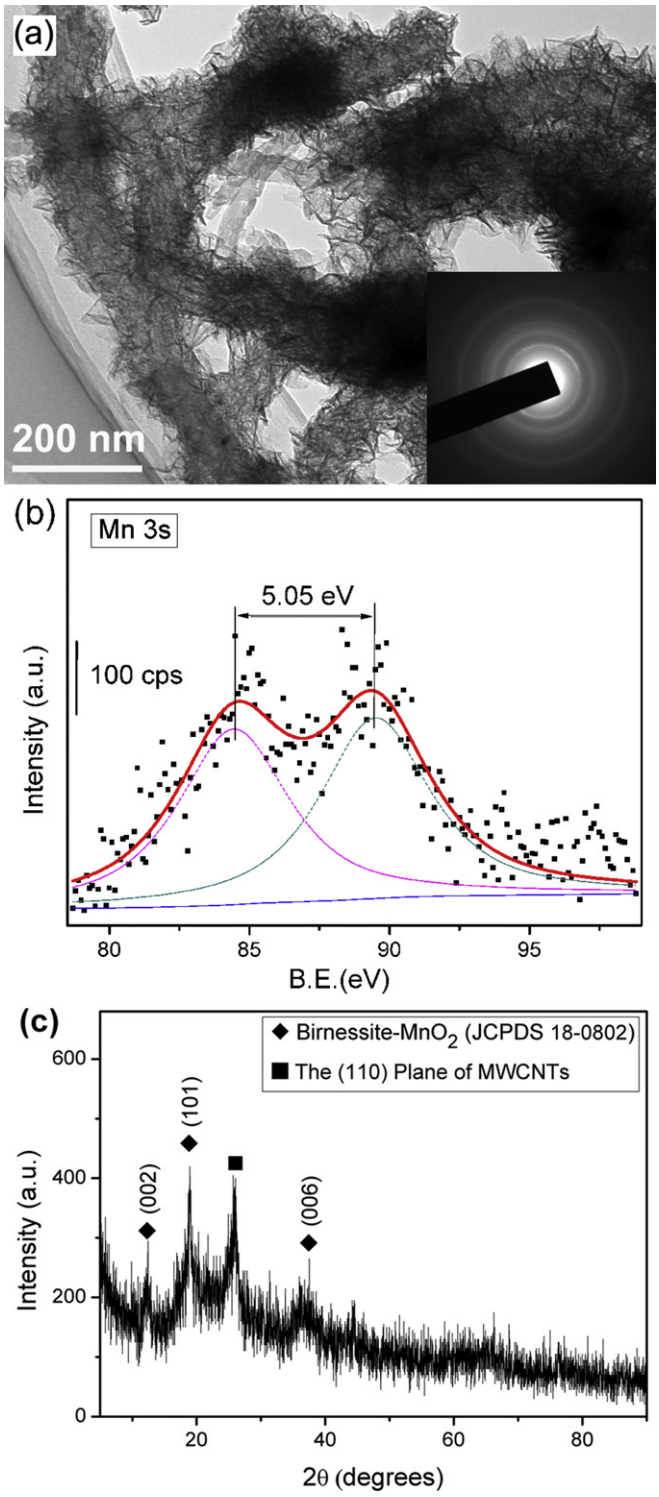

Fig. 8. Characterization results of the MMCNC films which have undergone the 1200 GCD cycle test. (a) TEM image (inset shows the SAED pattern of manganese oxide sheath), (b) Mn 3s XPS spectra and (c) XRD pattern.

electrode active material/electrolyte interface and thus larger capacitance, which can explain the slightly capacitance rise during the GCD cycles.

The above mentioned superior capacitive performances obtained from the MMCNC films are far better than that of the recently reported γ-MnOOH nanorods (132 F g^{-1} at a GCD current density of 0.5 A g^{-1}) [9] and MnOOH nanowire–graphene oxide composites (76 F g^{-1} at a GCD current density of 0.1 A g^{-1}) [10]. In addition to their higher specific capacitance, the MMCNC films also show excellent power performance. The improvement in capacitive performances can be attributed to the structural advantages of the MMCNC films. On one hand, the 1D coaxial nanocable structure works. Specifically, the MWCNT core can provide conductive frame for the electron transfer to the α-MnOOH sheath, while, the α-MnOOH sheath can provide high pseudocapacitance. On the other hand, the 3D nanoporous network structure can reduce the migration distance and diffusion resistance of the electrolyte ions in the MMCNC films during the GCD process. Based on the above mentioned structural advantages, excellent capacitive performances can be expected from the MMCNC films.

3.6. Charge storage mechanism

To study the charge storage mechanism, the MMCNC electrodes which had undergone the GCD cycle test were further characterized by TEM, XPS and XRD measurements. Typical TEM image of the MMCNCs which have experienced 1200 GCD cycles is shown in Fig. 8a. Compared with Fig. 2c and d, obvious morphology change is happened. The oxide sheath is transformed into nanoflakes from the nanosized microcrystals after experiencing the 1200 GCD cycles. Fortunately, the nanoflakes are still attached to the sidewall of the MWCNTs and the core/sheath microstructure of the 1D coaxial nanocables remains stable, which is very crucial for the long cycle life stability of the MMCNC electrodes. However, as shown in the inset of Fig. 8a, the MMCNC films undergone the 1200 GCD cycles show different SAED pattern compared with that of the pristine MMCNC films shown in the inset of Fig. 2c, indicating the crystal phase change in the GCD process.

XPS spectroscopy was carried out to check the oxidation state change of manganese element during the GCD cycles. As shown in Fig. 8b, the ΔE of Mn3s is reduced to 5.05 eV after the GCD cycle test. The calculated valence of Mn atoms is increased to ~3.3, indicating the likely coexistence of MnOOH and MnO_2 phase in the MMCNC films which have experienced the GCD cycle test. The generation of MnO_2 phase can be further demonstrated by the XRD measurement. As shown in Fig. 8c, there are new diffraction peaks emerged from the MMCNC films which have experienced the GCD tests. These broad XRD peaks centered at $2\theta = 12.28^\circ$, 18.67° and 36.81° can be well indexed to the (002), (101) and (006) planes of birnessite-MnO_2 (JCPDS 18-0802), respectively. It can be inferred that some of the MnOOH sheath is transformed into birnessite-MnO_2 phase after the 1200 GCD cycles. The above mentioned characterization results can corroborate the previously reported charge storage mechanism of MnOOH as follows [9]:

$$MnOOH \Leftrightarrow MnO_2 + H^+ + e^- \quad (4)$$

$$MnO_2 + Na^+ + e^- \Leftrightarrow MnOONa \quad (5)$$

3.7. Effect of film mass loading on the areal capacitance

For practical application of film electrodes in supercapacitors, it is very useful to increase the areal capacitance by increasing the areal mass loading of active materials [15,39]. Fortunately, the areal mass loading of the films prepared by EPD technique can be easily adjusted by altering the deposition time [16,17]. Thus, EPD experiments with extended deposition time ranging from 30 to 900 s were carried out to tune the mass loading and areal capacitance. As shown in Fig. 9d, the areal mass loadings increase linearly as the increase of deposition time, from 0.05 mg cm^{-2} at 30 s to 1.38 mg cm^{-2} at 900 s. Accordingly, the film thickness increase from 2.5 μm at 150 s to 15 μm at 900 s, as shown in the inset of Fig. 9d. It

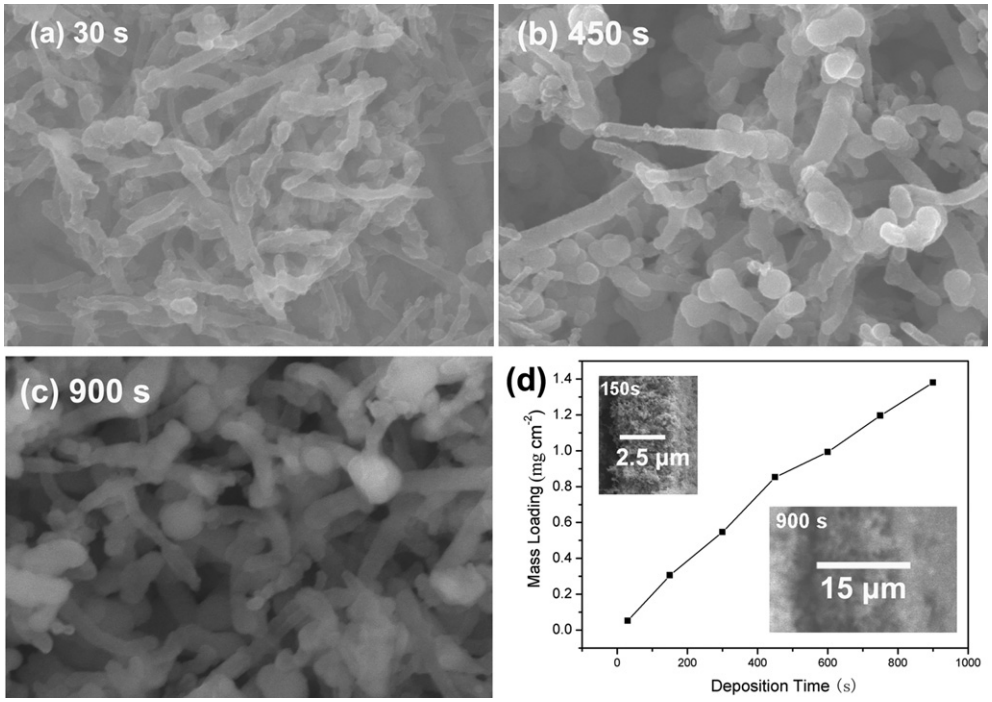

Fig. 9. The typical surface SEM images of the MMCNC films obtained at (a) 30 s, (b) 450 s, (c) 900 s; and (d) areal mass loading vs. deposition time plot (inset shows the cross-section SEM images of the MMCNC films obtained at 150 s and 900 s, respectively).

is worthwhile to point out that the 3D nanoporous morphologies of the MMCNC films show no significant change as the deposition time ranging between 30 s and 900 s based on the SEM images shown in Fig. 9a, b and c.

GCD tests were carried out to study the impact of mass loading on the capacitive performances of the MMCNC films. The specific capacitance vs. GCD current density plots for the MMCNC films with different areal mass loadings are shown in Fig. 10a. As the GCD current density increases, the capacitance shows a general trend of decrease for all the MMCNC films. At a fixed GCD current density, the mass specific capacitance reveals a declining trend as the mass loading increases, which might be resulted from the larger diffusion resistance of electrolyte ions and increased electron transport resistance in the thicker films. The highest specific capacitance of 327 F g^{-1} is obtained from the thinnest MMCNC film with a mass loading of 0.05 mg cm^{-2} at a current density of 0.2 mA cm^{-2}.

The dependence of areal capacitance on the areal mass loading of the MMCNC film is plotted in Fig. 10b. At the relatively low GCD current density of 0.2 mA cm^{-2}, the areal capacitance reveals a general upward trend with the increase of the areal mass loading. When the areal mass loading is increased to 1.38 mg cm^{-2}, the areal capacitance reaches a relatively high value of 0.2 F cm^{-2}, while maintaining a relatively high mass specific capacitance of 137 F g^{-1} (see Fig. 10a). When at high GCD current density of 5 mA cm^{-2}, the areal capacitance reaches a peak value of 0.06 F cm^{-2} from the films with a moderate areal mass loading of 0.99 mg cm^{-2}.

Based on the above mentioned data, the thickness, mass loading and capacitive performances of the MMCNC films can be easily and continuously tuned within a certain range by varying the deposition time. Considering the very simple and effective synthetic process, the MMCNC films with relatively high areal capacitance are competitive candidate for supercapacitor application.

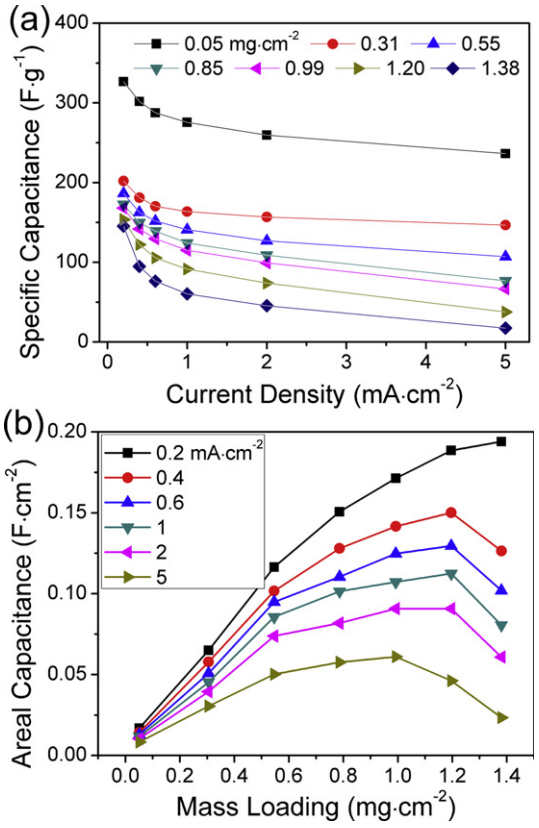

Fig. 10. (a) Mass specific capacitance vs. GCD current density plots for the MMCNC films with different areal mass loadings; (b) areal capacitance vs. MMCNC areal mass loading plots at different GCD current densities.

4. Conclusions

As far as we are aware, this is the first time that EPD technique has been used for one-step fabrication of a coaxial nanocable structure. During the reported EPD process, the cathodic deposition of $Mn(OH)_2$ on the sidewall of the MWCNT is occurred synchronously with the deposition of MWCNTs on nickel foils, resulting in uniform $Mn(OH)_2$ coatings on the MWCNT frame through the entire film thickness. Subsequent oxidation of the $Mn(OH)_2$ leads to the formation of the MMCNC films.

Due to their 3D nanoporous network structure composed of 1D MMCNCs, the as-prepared MMCNC films show excellent capacitive performances and long cycle life stability. It is worth mentioning that the thickness, mass loading and capacitive performances of the MMCNC films can be easily and continuously tuned by changing the deposition time. Consequently, the reported MMCNC films could be a qualified candidate for supercapacitor application. The synthetic method presented here is very simple and effective, and may be extended to fabricate other coaxial nanostructures for future electrochemical energy storage devices combining high power and high energy densities.

Acknowledgments

This work was supported by the National Basic Research Program of China (973 Program) (2013CB934001), National Natural Science Foundation of China (51074011 and 51274017) and National 863 Program (2007AA03Z231 and 2011AA11A257). Dr. Ruoxu Lin and Dr. Ye Lin are gratefully acknowledged for performing the SEM measurement.

References

[1] P. Simon, Y. Gogotsi, Nat. Mater. 7 (2008) 845–854.
[2] G. Wang, L. Zhang, J. Zhang, Chem. Soc. Rev. 41 (2012) 797–828.
[3] Y. Zhang, H. Feng, X. Wu, L. Wang, A. Zhang, T. Xia, H. Dong, X. Li, L. Zhang, Int. J. Hydrogen Energy 34 (2009) 4889–4899.
[4] A. Ghosh, Y.H. Lee, ChemSusChem 5 (2012) 480–499.
[5] W. Chen, R.B. Rakhi, L. Hu, X. Xie, Y. Cui, H.N. Alshareef, Nano Lett. 11 (2011) 5165–5172.
[6] Q. Qu, S. Yang, X. Feng, Adv. Mater. 23 (2011) 5574–5580.
[7] G.-R. Li, Z.-P. Feng, Y.-N. Ou, D. Wu, R. Fu, Y.-X. Tong, Langmuir 26 (2010) 2209–2213.
[8] J. Lang, X. Yan, Q. Xue, J. Power Sources 196 (2011) 7841–7846.
[9] Z. Li, H. Bao, X. Miao, X. Chen, J. Colloid Interface Sci. 357 (2011) 286–291.
[10] L. Wang, D.-L. Wang, Electrochim. Acta 56 (2011) 5010–5015.
[11] K.-W. Nam, C.-W. Lee, X.-Q. Yang, B.W. Cho, W.-S. Yoon, K.-B. Kim, J. Power Sources 188 (2009) 323–331.
[12] I.-H. Kim, J.-H. Kim, B.-W. Cho, K.-B. Kim, J. Electrochem. Soc. 153 (2006) A1451–A1458.
[13] B. Wen, S. Zhang, H. Fang, W. Liu, Z. Du, Mater. Chem. Phys. 131 (2011) 8–11.
[14] S.L. Chou, J.Z. Wang, S.Y. Chew, H.K. Liu, S.X. Dou, Electrochem. Commun. 10 (2008) 1724–1727.
[15] L. Hu, W. Chen, X. Xie, N. Liu, Y. Yang, H. Wu, Y. Yao, M. Pasta, H.N. Alshareef, Y. Cui, Acs Nano 5 (2011) 8904–8913.
[16] I. Corni, M.P. Ryan, A.R. Boccaccini, J. Eur. Ceram. Soc. 28 (2008) 1353–1367.
[17] B.J.C. Thomas, A.R. Boccaccini, M.S.P. Shaffer, J. Am. Ceram. Soc. 88 (2005) 980–982.
[18] J. Li, I. Zhitomirsky, J. Mater. Process. Tech. 209 (2009) 3452–3459.
[19] Y. Wang, I. Zhitomirsky, Langmuir 25 (2009) 9684–9689.
[20] Y. Wang, I. Zhitomirsky, Colloid Surf. A 369 (2010) 211–217.
[21] W. Xiao, H. Xia, J.Y.H. Fuh, L. Lu, Phys. Scr. T139 (2010) 014008.
[22] J. Zhang, Y. Wang, J. Zang, G. Xin, Y. Yuan, X. Qu, Carbon 50 (2012) 5196–5202.
[23] C.S. Du, N. Pan, Nanotechnology 17 (2006) 5314–5318.
[24] M.S. Wu, C.Y. Huang, K.H. Lin, Electrochem. Solid-State Lett. 12 (2009) A129–A131.
[25] J. Lu, Carbon 45 (2007) 1599–1605.
[26] S. Santhanagopalan, F. Teng, D.D. Meng, Langmuir 27 (2011) 561–569.
[27] J.W. Liu, J. Essner, J. Li, Chem. Mater. 22 (2010) 5022–5030.
[28] T.E. Moore, M. Ellis, P.W. Selwood, J. Am. Chem. Soc. 72 (1950) 856–866.

[29] Z.-R. Tian, W. Tong, J.-Y. Wang, N.-G. Duan, V.V. Krishnan, S.L. Suib, Science 276 (1997) 926–930.
[30] X.H. Feng, F. Liu, W.F. Tan, X.W. Liu, Clays Clay Miner. 52 (2004) 240–250.
[31] D. Liu, B.B. Garcia, Q. Zhang, Q. Guo, Y. Zhang, S. Sepehri, G. Cao, Adv. Funct. Mater. 19 (2009) 1015–1023.
[32] D. Liu, Q. Zhang, P. Xiao, B.B. Garcia, Q. Guo, R. Champion, G. Cao, Chem. Mater. 20 (2008) 1376–1380.
[33] T. Gao, P. Norby, F. Krumeich, H. Okamoto, R. Nesper, H. Fjellvåg, J. Phys. Chem. C 114 (2010) 922–928.
[34] W. Sun, A. Hsu, R. Chen, J. Power Sources 196 (2011) 627–635.
[35] T. Gao, F. Krumeich, R. Nesper, H. Fjellvåg, P. Norby, Inorg. Chem. 48 (2009) 6242–6250.
[36] H.W. Nesbitt, D. Banerjee, Am. Mineral. 83 (1998) 305–315.
[37] E.N. Konyushenko, J. Stejskal, M. Trchová, J. Hradil, J. Kovářová, J. Prokeš, M. Cieslar, J.-Y. Hwang, K.-H. Chen, I. Sapurina, Polymer 47 (2006) 5715–5723.
[38] B. Folch, J. Larionova, Y. Guari, C. Guérin, C. Reibel, J. Solid State Chem. 178 (2005) 2368–2375.
[39] M.D. Stoller, R.S. Ruoff, Energy Environ. Sci. 3 (2010) 1294–1301.